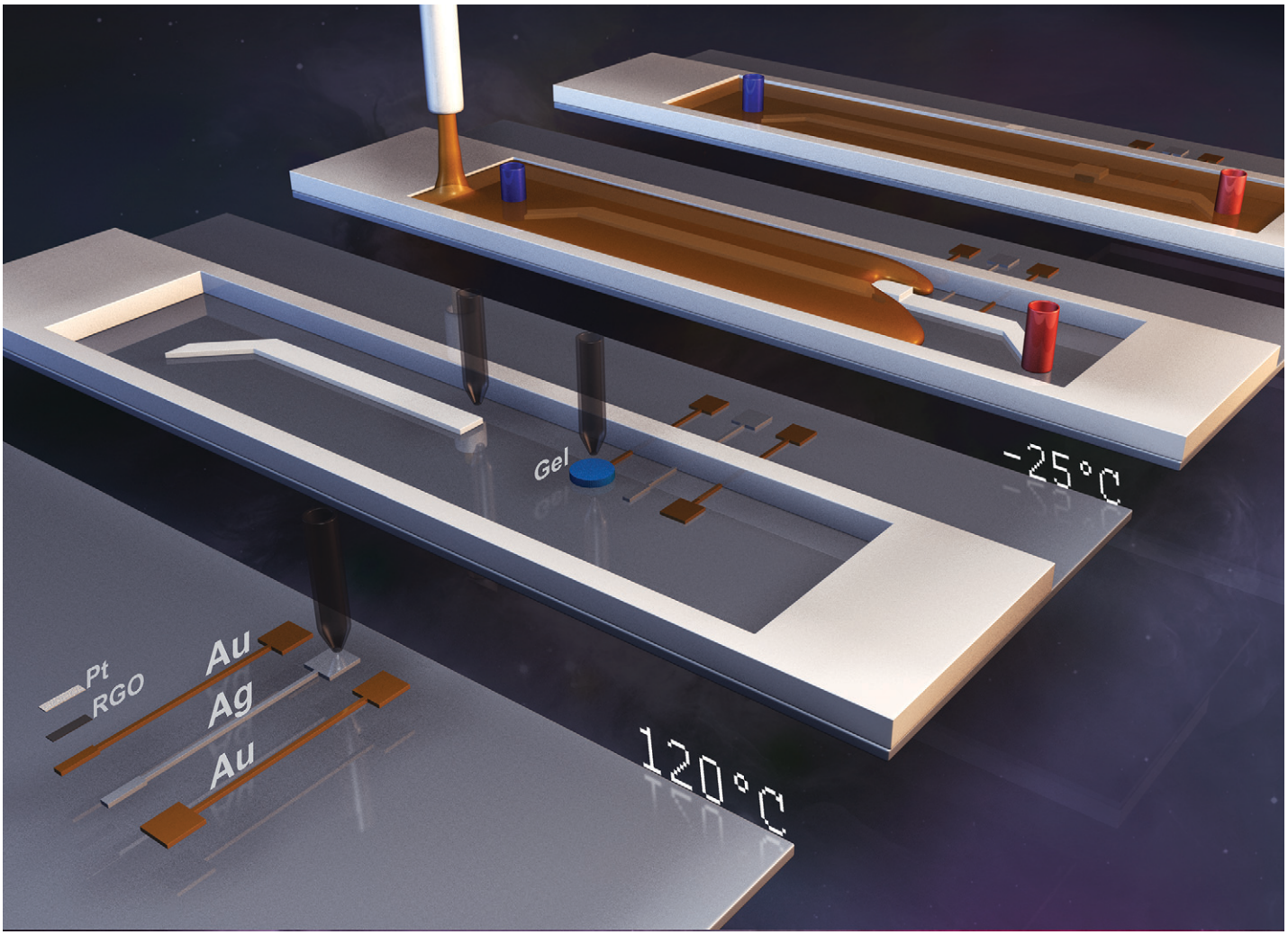

Featuring work from Zhihong Li's group at the National Key Laboratory of Science and Technology on Micro/Nano Fabrication, Institute of Microelectronics, Peking University, China.

From functional structure to packaging: full-printing fabrication of a microfluidic chip

A full-printing process based on layer-by-layer inkjet printing is developed to achieve a cost-effective and time-saving fabrication method. A glucose detection microfluidic chip sensor is successfully fabricated by this method, which shows good sensitivity and a linear section at a low concentration of glucose (0–10 mM).

As featured in:

See Dachao Li, Zhihong Li *et al.*, *Lab Chip*, 2018, **18**, 1859.

ROYAL SOCIETY OF CHEMISTRY

rsc.li/loc

Registered charity number: 207890

Lab on a Chip

PAPER

View Article Online
View Journal | View Issue

Cite this: *Lab Chip*, 2018, **18**, 1859

From functional structure to packaging: full-printing fabrication of a microfluidic chip†

Fengyi Zheng, ‡[a] Zhihua Pu, ‡[b] Enqi He,[ac] Jiasheng Huang,[a] Bocheng Yu,[a] Dachao Li*[b] and Zhihong Li*[a]

Received 30th March 2018,
Accepted 18th May 2018

DOI: 10.1039/c8lc00327k

rsc.li/loc

This paper presents a concept of a full-printing methodology aiming at convenient and fast fabrication of microfluidic devices. For the first time, we achieved a microfluidic biochemical sensor with all functional structures fabricated by inkjet printing, including electrodes, immobilized enzymes, microfluidic components and packaging. With the cost-effective and rapid process, this method provides the possibility of quick model validation of a novel lab-on-chip system. In this study, a three-electrode electrochemical system was integrated successfully with glucose oxidase immobilization gel and sealed in an ice channel, forming a disposable microfluidic sensor for glucose detection. This fully-printed chip was characterized and showed good sensitivity and a linear section at a low-level concentration of glucose (0–10 mM). With the aid of automatic equipment, the fully-printed sensor can be massively produced with low cost.

Introduction

Microfluidics technology has great impacts on a broad range of areas from biological analysis to chemical synthesis.[1] Microfluidic devices based on lab-on-a-chip (LOC) possess the advantages of rapid analysis, increased automation, low power consumption, ease of operation, integration capability of multiplexing analysis, and compatibility with mass production.[2] LOC enables significant advancement in chemical and biochemical analysis owing to advances in physics, electronics and materials science.[3] In terms of fabricating or replicating microchannel structures, the dominant techniques utilized in microfluidics can be divided into three main categories: bulk micromachining, surface micromachining and mould machining.[4] Typically, expensive equipment is necessary for photolithography, deposition and etching in the first two categories, while the third one is strongly dependent on master mould fabrication, which normally needs significantly expensive and time-consuming techniques. However, the high expense and long period fabrication process, on a certain extent, go against the research and development of designing new microfluidic devices. More importantly, for most biological uses, microfluidic devices are embedded with biofunctional materials such as DNAs, antibodies, enzymes, and hydrogels, which are delicate and prone to damage or contamination by microfabrication processes such as photolithography,[5] chemical reduction,[6] evaporation,[7] sputtering,[8] lift-off,[9] bonding,[10] thermal annealing,[11] plasma treatment,[12] *etc.* Therefore, fixation *via* double-sided adhesive tape,[13] or clamps,[14] which is complicated and at high risk of leakage, is required to construct microchannels or reservoirs enclosing biofunctional materials. Alternatively, surface modification and biomolecule immobilization are carried out after microfluidic structure formation. However, the required biochemical reaction in a long microchannel is time consuming with low efficiency.

In recent years, the up-and-coming inkjet printing technology has been arguably the most promising option to address the aforementioned limitations.[15] In this additive manufacturing, only the areas needed to be patterned are coated and the process requires no stamp or mask. Besides, the ability to print multiple materials, individually and simultaneously, offers great flexibility while designing. Inkjet printing has been proved to be best used in combination with other manufacturing techniques and shows good prospects for the development of fully inkjet-printed electrochemical sensors.[16]

In our previous work, we successfully achieved an additive method for microelectrode patterning using silver nanoparticles on a PDMS substrate[17] and graphene modification on the surface of a working electrode on a polyimide

[a] *National Key Laboratory of Science and Technology on Micro/Nano Fabrication, Institute of Microelectronics, Peking University, Beijing 100871, China. E-mail: zhhli@pku.edu.cn*
[b] *State Key Laboratory of Precision Measuring Technology and Instruments, Tianjin University, Tianjin 300072, China. E-mail: dchli@tju.edu.cn*
[c] *State Key Laboratory of Tribology, Department of Mechanical Engineering, Tsinghua University, Beijing 100084, China*

† Electronic supplementary information (ESI) available: See DOI: 10.1039/c8lc00327k

‡ Fengyi Zheng and Zhihua Pu contributed equally to this work.

substrate.[18] These two works showed tight bonding between patterns and substrates and good combination between different layers of patterns. The electrodes also presented good electroactivity and achieved a significantly uniform distribution of electrochemical active sites on the WE surface. On the other hand, a fabrication technology called 3D ice printing was proposed to provide a bio-friendly method for chemical biosensor fabrication.[19] The process environment of 3D ice printing with low temperature and nitrogen atmosphere was beneficial to enzyme immobilization in hydrogel.[20] Based on inkjet-printed electrode technology and 3D ice-printing technology, we pioneer a full-printing fabrication method, aiming at fabricating the whole structure of lab-on-a-chip and microfluidic devices by inkjet printing with aqueous solution of different materials as ink. This method endows ice sacrificial layers with not only the indicating solution but also the protective layer of biological samples pre-sealed in the chip. Graphics of different materials and structures are designed in the same coordinate system layer-by-layer using CAD software to achieve alignment. Consequently, more sophisticated 3D ice structures with fine feature sizes and even enzyme embedded gel patterns can be integrated by processing the layer-by-layer printing sequences. On the basis of our proposed full-printing method, we successfully fabricate a glucose detection microfluidic chip as a significant supplement to our previous work.[18,21] This fully printed chip shows good sensitivity and a linear section at a low-level concentration of glucose (0–10 mM). With the aid of automatic equipment, this kind of chip can be massively and cost-effectively produced and enables the evolution of highly efficient and versatile analytical tools in the biomedical field.

Principle

In this paper, we take a glucose detection sensor as an example for the full-printing fabrication method. Fig. 1(a) demonstrates the schematic view of the designed sensor, which consists of a testing area, a straight ice channel acting as microfluidics for sample injecting and a photopolymer as an encapsulation layer. The testing area and the microfluidics are entirely fabricated by inkjet printing. As shown in Fig. 1(b), the structure of the testing area has three layers, including a three-electrode system, a piece of immobilized glucose oxidase gel, and an ice structure channel connected with the microfluidics. Both the working electrode and the reference electrode are 200 μm × 1000 μm, and the counter electrode is 1000 μm × 1000 μm. All the three leads are 100 μm × 5000 μm and the pads are 1000 μm × 1000 μm. The gel with immobilized enzymes acts as an electrochemically sensing material and covers the WE. A 500 μm width ice line, printed by the ice printing technique, runs through the gel and forms a 300 μm height microfluidic channel after the solidification of a 2 mm thick sealing photopolymer. The low-temperature environment during the fabrication process and the preservation protects the biological activity of the glucose oxidase. When it comes into testing at room temperature, the ice structure melts and forms a channel with buffer in it. The glucose solution fully fills the microfluidic channel and diffuses into the porous structure of the hydrogel to conduct the catalytic reaction. The electric current of reaction can be detected using an ammeter connected with the leads of the electrodes.

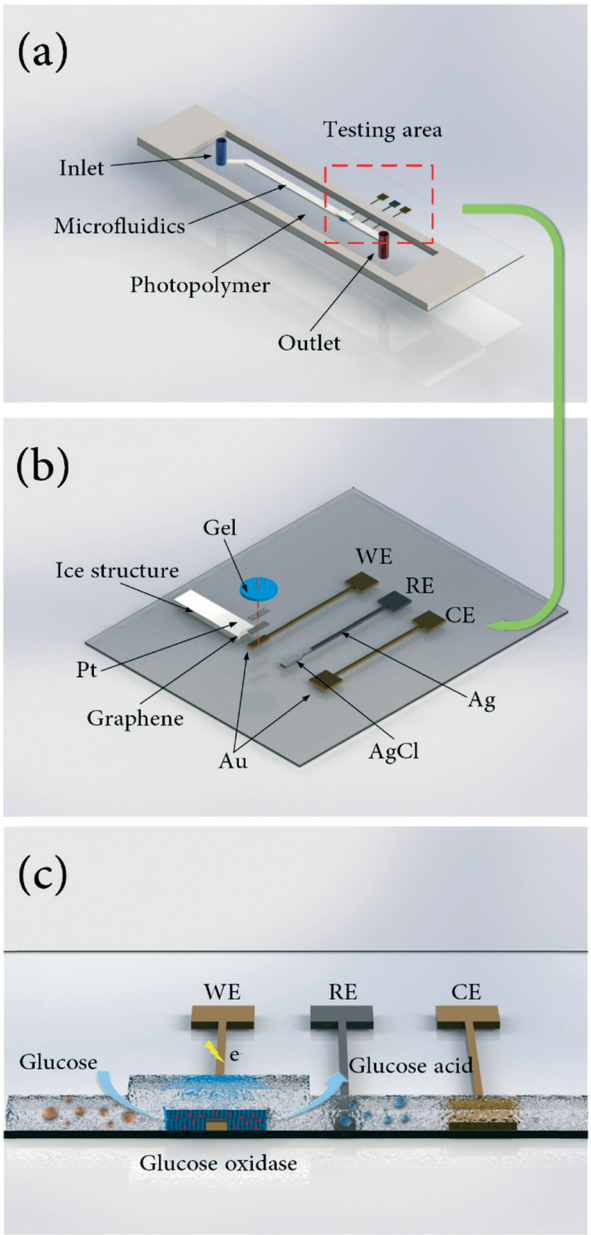

Fig. 1 The schematic view of a full-printing glucose sensor. (a) The complete sensor; (b) details of the printed structure. (c) Schematic diagram of the electrochemical sensor for glucose measurement and its integration into a full-printing chip.

Method

Printing system

Two self-built printing systems, an ice-printing system as shown in Fig. 2 and a nanomaterial printing system similar to that shown in a previous work,[18] are used together to enable

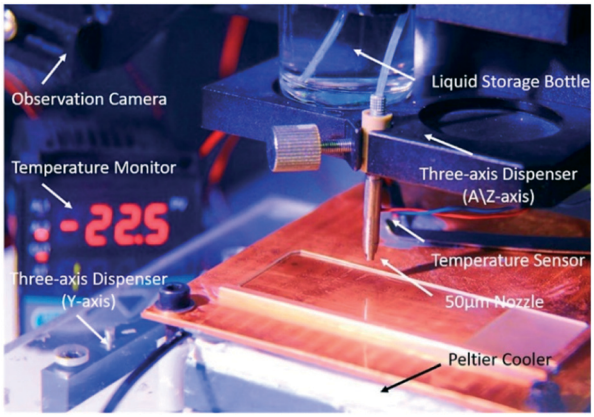

Fig. 2 The self-built ice-printing system.

the fabrication of the proposed full-printing microfluidic chip. The two self-built printing systems consist of four parts: the printing module, the three-axis mobile robot, the temperature control system and the observation module. The printing module, made up of piezoelectric printheads (one with a nozzle diameter of 50 μm for the ice-printing system and four with a nozzle diameter of 30 μm for the nanomaterial printing system), an electric controller and waveform control software, is purchased from MicroFab Technologies, Inc., USA.

The three-axis mobile robot is custom-made from Ruidu Photoelectric, Inc., Shanghai, which provides the conversion software for CAD graphics to an execution program, the three-dimensional movement, and the localization of the position relationship between the nozzle and the substrate. The temperature control system consists of two subsystems, a hot plate for heating and a Peltier cooler for freezing (the nanomaterial printing system contains only a hot plate while the ice-printing system contains both of them). The two subsystems are both covered with a latten to ensure the evenness of temperature on the surface of the substrate. The temperature is monitored using a Pt-1000 thermistor connected with a digital temperature meter. The observation module includes a diagonally positioned camera and a strobe, which allows us to observe the printing status as well as calibrate the start-point for printing.

Similar to the previous ice-printing work we have conducted in 2015, we put the whole ice-printing system in a airtight glove box to control the humidity and the oxygen content by adjusting the influx and outflow rates of nitrogen. Low humidity contributes to the shape maintenance of the ice printing pattern. Isolation of oxygen is necessary for copolymerization of most gels.

The pattern control of nanoparticle printing

Different nanomaterials require different parameters for printing, including the voltage of the piezoelectric nozzle, the space between each printed droplet and the temperature of the substrate. Firstly, nanomaterial ink with high viscosity needs a higher peak-to-peak value of voltage to generate regular droplets without satellites. Secondly, ink with high viscosity also needs a bigger space between the droplets on the substrate because the diameter of the droplet will get bigger when it crashes onto the substrate[22] and the viscous liquid changes more significantly. In order to form a smooth edge, the droplets should always fall on the circumference of the prior imprinting marks. The empirical estimates of the size of the droplets for Au nanoparticles and Ag nanoparticles on glass slides are 95 μm and 65 μm. Thirdly, ink with high viscosity needs a relatively low substrate temperature to reach a lower rate of evaporation as it takes a longer time for the droplets to come onto the film driven by surface tension.[23] Our experiments show that the suitable time and temperature for Au are 30 minutes and 200 °C and for Ag are 10 minutes and 220 °C.

Generally, the film formed by nanoparticles of Au/Ag/graphene needs postbaking at a higher temperature to make the nanoparticles achieve a secondary fusion, which will markedly enhance the compactness of the film and the adhesion to the substrate. The temperature and time of postbaking depend on the material of nanoparticles.

The challenge of ice-printing in microfluidic fabrication

Here we improve the ice printing ability of our previous work to make the ice structure customizable and usable for graphical representations of functional microfluidics. The major challenge in the development of the full-printing method is controlling three-dimensional structures of ice, which is mainly influenced by the space between every two droplets l. As the printing frequency f and the velocity of the nozzle v are the only two parameters we are able to control in the software, the key is to find the specific relationship between l, v and f. When a line segment of L in length is made up of n droplets, it is obvious that l equals L divided by n. The number of droplets n equals f multiplied by the printing time t, while t equals the distance L divided by the velocity of the nozzle v. According to the above-mentioned relationship, we obtain the following equation between l and the ratio of velocity to frequency:

$$l = \frac{L}{n} = \frac{L}{f \cdot t} = \frac{L}{f \cdot L/v} = \frac{v}{f}$$

Affected by surface tension, the droplets on the surface of the substrate will gather into a bigger droplet when l is smaller than its diameter d. The bigger the droplet is, the slower it is to freeze into ice, and then the bigger liquid phase droplet will adsorb other small droplets. Meanwhile, when l is too big, the line segment will be discontinuous instead of the designed shape. Experimental results demonstrate that the appropriate l_0 is between $0.7d$ and $1.2d$, considering the height reduction of the edge of the ice pellets and the volume expansion during the freezing process.

Another challenge is the supercooling water phenomenon. Supercooling is the process of lowering the temperature of a

liquid or a gas below its freezing point without solidification. In our work, we find that microdroplets crashing onto the cold surface are easy to freeze while large droplets more likely become an amorphous (non-crystalline) solid. Meanwhile, a liquid crossing its standard freezing point will crystallize in the presence of a seed crystal or nucleus around which a crystal structure can be formed through solidification. Thus the ice patterns must be printed in two steps. We first set the printing process at low frequency to make the microscale droplets arranged in lines quickly freeze into an ice trace. The ice trace acts as an ice nucleus in the second printing process to avoid the supercooling phenomenon. As the second printing process is at a high printing frequency, the ice structure is filled up fast in the *z*-axis.

Experimental

Chemicals

Gold nanoparticle ink was bought from UT Dots, Inc., USA. Silver nanoparticle ink and reduced graphene oxide (RGO) ink were purchased from Sigma Aldrich. Platinum nanoparticle ink was obtained from Changchun Institute of Applied Chemistry, Chinese Academy of Sciences. Glucose oxidase (GOx, type X-S, lyophilized powder, 100 units per mg), acrylamide and *N*,*N*-methylenebis-acrylamide were obtained from Sigma-Aldrich (St. Louis, MO). Riboflavin, potassium, sodium chloride (NaCl), sodium phosphate dibasic dodecahydrate ($Na_2HPO_4{\cdot}12H_2O$), monobasic potassium phosphate (KH_2PO_4) and potassium chloride (KCl) were purchased from Beijing Chemicals (Beijing, China).

Other equipment and materials we used are as follows: a Peltier cooler, digital thermometer and hygrometer, light cure medical adhesive (Loctite 3311), clear float glass slides, and poly(methyl methacrylate) (PMMA).

Fig. 3 demonstrates the schematic view of the fabrication process of the full-printing method, which could be divided into four steps according to the temperature variation of the substrate. The optical photograph of the completed chip is illustrated in Fig. 4(a).

Printing and modification of the electrodes

First of all, a float glass slide was cleaned with ethyl alcohol and treated with corona. Then the substrate was heated to 120 °C using a hot plate and the three electrodes of the electrochemical biosensor were inkjet printed on it. The printing process consisted of three steps, as shown from Fig. 3(a)–(c). Firstly, the nano-gold ink was printed to form the working electrode and the counter electrode. These two electrodes required a postbaking process for fifteen minutes at 210 °C. Secondly, the nano-silver ink was patterned as the reference electrode and was postbaked for ten minutes at 210 °C. Next, ferric chloride was dropped onto the pad of the reference electrode for twenty seconds to complete the chlorination and then was washed away with ultrapure water. Thirdly, the RGO ink was sprayed onto the pad of the working electrode to improve the detection of weak glucose signals, and the Pt nanoparticle solution was printed on the layer of RGO to enhance the electron-mobility of the electrode.[18] The layers of Au and Pt were printed twice to ensure that the film of the electrode had no flaw of holes and the layer of graphene was just printed once.

Printing and immobilization of enzymes on the working electrode

Table 1 shows the components of the required solution. 0.1 M standard phosphate buffer (PBS, pH = 7.4) was prepared by dissolving 8 grams of NaCl, 2.89 grams of $Na_2HPO_4{\cdot}12H_2O$, 0.2 grams of KH_2PO_4 and 0.2 grams of KCl in 1 L of ultrapure water. All the solutions were diluted with PBS and were used right after they were ready. The gel was prepared by mixing 1 mL of the stock solution of the monomer with 4 mL of the crosslinking reagent. The reagent mixture was deoxygenated in a vacuum air-removed pot before the addition

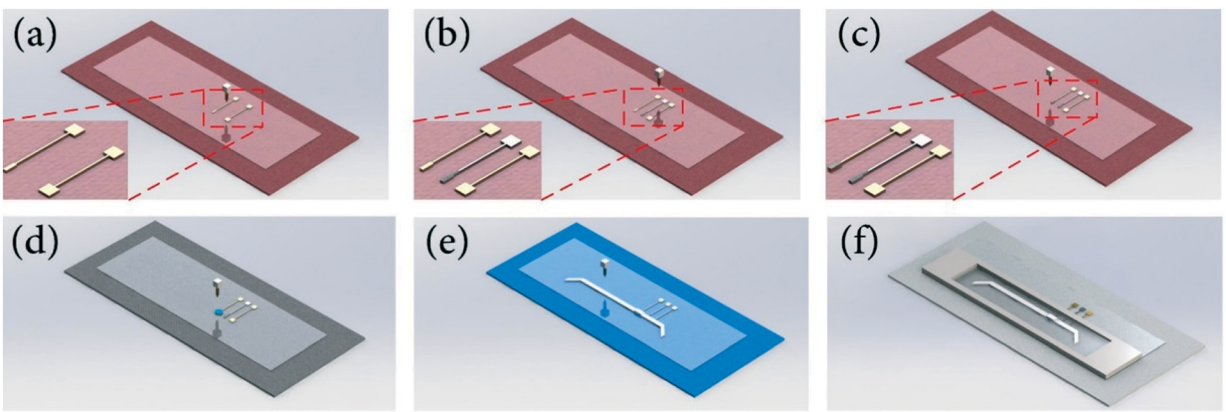

Fig. 3 Fabrication process of the full-printing glucose sensor. (a) Printing of the Au patterns, including the first layer of the working electrode (left) and the counter electrode (right); (b) printing of the Ag patterns, which act as the reference electrode. $FeCl_3$ was dropped onto one side of the electrode for 20 seconds to form AgCl; (c) printing of GOx and Pt to finish the modification of the working electrode; (d) printing of the glucose oxidase embedded gel; (e) printing of the ice channel; (f) packaging using a photopolymer.

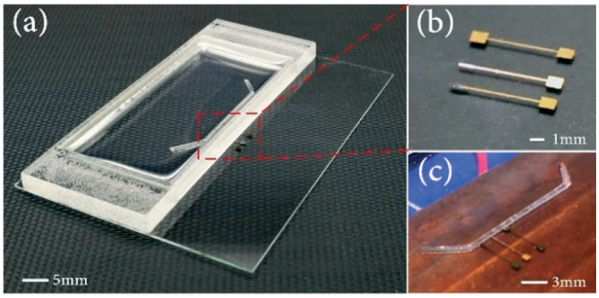

Fig. 4 (a) The completed glucose detection chip. (b) The detail of the printed electrodes. (c) The detail of the ice structure running through the electrodes.

of the glucose enzyme to avoid the oxygen inhibition of the copolymerization. Then 1 mL of enzyme solution, 100 μL of a photocatalyst and 100 μL of a crosslinking catalyst were added into the gel solution, respectively. Because the small volume of potassium persulfate was not able to catalyse the polymerization while a further quantity of the initiator would harm the enzyme activity, the photoinitiator was combined with potassium persulfate to make a balance between the speed of catalysis and the preservation of biological activity.

The pattern of the gel solution was designed in a circular shape with a diameter of 500 μm, which totally covered the pad of the working electrode. As the operation box was full of nitrogen, the anaerobic copolymerization proceeded rapidly when it was exposed to a 365 nm LED (7 watts) and was completed in twenty minutes, with the end point defined as the time taken for the gel to reach maximum opacity. The wavelength of 365 nm belonged to ultraviolet A (UVA). On the one hand, the penetrability of UVA was weak and its half-life period was much shorter in the water-diluted solution than in air. So it will only do little damage to the enzyme. On the other hand, the activity of the enzyme depended on its active site. Enzyme immobilization in gel benefited the stability of the enzyme structure. Compared with the structural damage in the membrane structure with enzymes on the electrodes, the damage by UVA exposure was noteworthy (ESI† Fig. S1). Meanwhile, the temperature of the Peltier cooler was set to 0 °C to reduce the effect of heat denaturation of the enzyme during the exothermic reaction.

Printing and patterning of the ice channel

Next, the temperature of the Peltier cooler was adjusted to minus 25 °C. Ultrapure water was printed on the substrate and was frozen into the ice channel. The width of the ice channel, which ran through the circular disk of the gel, was designed to be 300 μm to avoid the movement of the gel in the microfluidic channel. As a single ice line formed by printing was about 150 μm, the ice channel was designed in two parallel segments with a gap of 150 μm.

The printing process was divided into two steps. First, we set the velocity of the nozzle to 6 mm s^{-1} and the frequency of the injection to 60 Hz with a circulation of five times in order to form the basic outline of the pattern. Then we printed the same pattern with a velocity of 20 mm s^{-1} and a frequency of 500 Hz with a circulation of ten times to make the structure of ice a higher-order structure. The height of the ice channel can reach 300 μm after the entire printing process.

Packaging of the sensor

Finally, a square cofferdam, which surrounded the area of the sensor, was placed on the substrate, and the photopolymer precursor was added and polymerized to seal the electrode, gel and ice channel. Compared with PDMS, light-sensitive adhesive had a fast curing speed and better adhesion to the substrate. Following consideration of the biocompatibility, transparency and Young's modulus, here we selected Loctite 3311, a medical grade light-sensitive adhesive, as a packaging material. Furthermore, Loctite 3311 has a low flowability in a low temperature environment and will not drain out of the cofferdam. Upon exposure to a 420 nm LED lamp (7 watts), the curing process was completed in three minutes at minus 25 °C.

Preservation and testing

The chip could be preserved at minus 4 °C to keep the biological activity of the glucose oxidase in the gel. Holes were punched at the start and the end of the microfluidic channel as the inlet and outlet when the chip was used at room temperature (22 °C). The reaction agent was injected into the chip through a flexible tube using a peristaltic pump. As the glucose oxidase was immobilized in the gel, the flowing solution did not come into contact with the enzyme directly. The catalytic reaction began when the glucose solution diffused into the porous structure of the gel. In this case velocity is not the main influence on the diffusion process when the microfluidic channel is fully filled. The bared pads of electrodes were connected to a galvanometer with copper wire fixed on them with conducting resin. The chip was

Table 1 The components of the gel embedding the enzyme

Function	Component	Concentration	Dosage
Stock solution of the monomer	Acrylamide	400 mg mL^{-1}	1 mL
Crosslinking reagent	*N*,*N*-Methylenebis-acrylamide	23 mg mL^{-1}	4 mL
Enzyme solution	Glucose oxidase	5 mg mL^{-1}	1 mL
Photocatalyst	Riboflavin	0.3 mg mL^{-1}	100 μL
Crosslinking catalyst	Potassium persulfate	0.3 mg mL^{-1}	100 μL

disposable as the fabrication method was cost-effective and can be massively produced easily.

Results and discussion

Characterization of electrodes

Physical characterization is illustrated from Fig. 5(a)–(c). Optical photographs and SEM images show that the printing method enables fabrication of a continuous uniform film. The energy spectrum (EDS) demonstrates that the medium arranges layer by layer as designed and has good stability and binding ability.

As shown in Fig. 5(d), the cyclic voltammetry characteristics of the three-electrode sensor satisfy the requirement of electrochemical detection in a microfluidics chip. Each layer of material printed on the WE surface was first tested using the amperometric technique. H_2O_2 was utilized to characterize the electrodes because it was generated as the decomposition of glucose by immobilized glucose oxidase (GOx). Fig. 5(e) shows the typical amperometric responses of the various sensor configurations to a successive increment of 0.5 mM H_2O_2 at an applied potential of −0.2 V. As shown in Fig. 5(e), the electrochemical response increases as the H_2O_2 concentration increases, and all of the sensors demonstrate

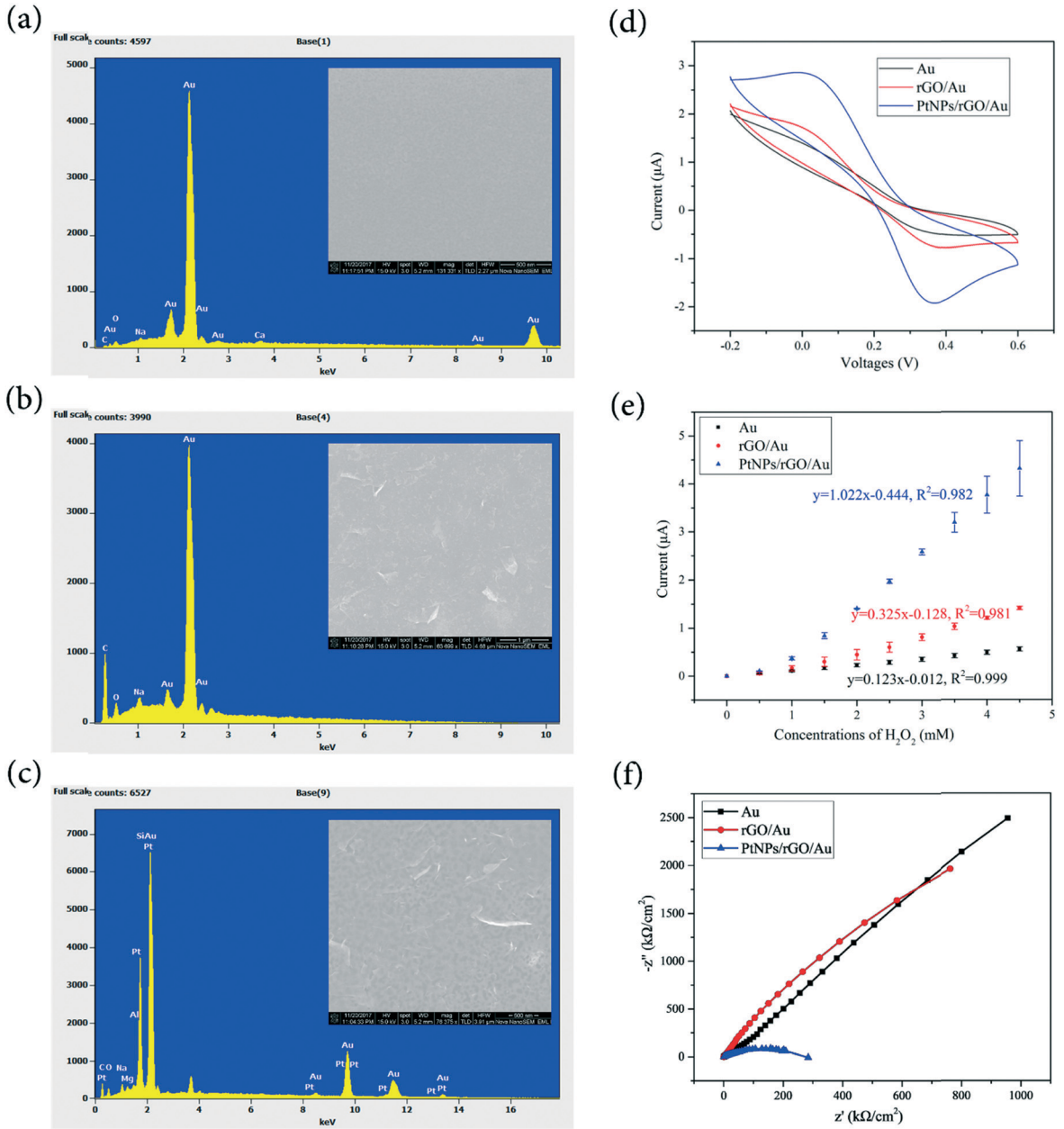

Fig. 5 Characterization of the electrodes. The optical photographs and SEM images of (a) Au; (b) graphene; and (c) Pt; (d) the cyclic voltammetry characteristics of the three-electrode sensor; (e) the typical amperometric responses of the various sensor configurations to a successive increment of 0.5 mM H_2O_2 at an applied potential of −0.2 V; (f) the Nyquist diagram of the EIS test for different configurations of the WE.

good linearity from 0 to 4.5 mM H_2O_2. Furthermore, the Nyquist diagram of the EIS test for different configurations of the WE is shown in Fig. 5(f), where 5 mM potassium ferricyanide ($K_3[Fe(CN)_6]$) in 0.1 M PBS was employed as the determinant, 500 mV DC and 10 mV AC potentials *vs.* Ag/AgCl were applied between the WE and CE with frequencies from 0.1 Hz to 100 kHz. Fig. 6 shows the equivalent electrical circuit model fitted using Zsimpwin. Rs, W, O, Rt, Ch and Cd represent the impedance of the solution between the WE and RE, the semi-infinite diffusion impedance of the WE, the finite layer diffusion impedance of the WE, the electron transfer resistance of the WE, the capacitance of the Helmholtz capacitor of the WE and the capacitance of the double-layer capacitor of the WE, respectively. The electron transfer rate significantly affected the sensitivity. According to the measured electrochemical impedance spectra and the obtained equivalent electrical circuit model, the Rt values of the three kinds of WEs were calculated to be 44.55 kΩ cm^{-2} (Au), 13.85 kΩ cm^{-2} (RGO/Au) and 0.13 kΩ cm^{-2} (PtNPs/RGO/Au). The WE with RGO and Pt nanoparticles held the smallest electrochemical impedance enhancing the electron transfer rate of the WE to satisfy low levels of glucose measurements.

Evaluation of the full-printing glucose sensor

In this paper, the sensitivity and the linearity of the glucose measurements were evaluated to prove that the fabrication of a full-printing biosensor was feasible. The interlayer of graphene improved the detection of weak glucose signals. Pt nanoparticles modified onto the WE surface improved the electroactive nature achieving a more uniform distribution of electrochemically active sites on the electrodes to enable measurements of glucose.[18] The detection limit was measured by successively increasing 0.01 mM glucose at an applied potential of 0.4 V and the first efficient signal was found at 0.05 mM. Then the experiments were conducted by detecting several representative points. Fig. 7 demonstrates the current signals of the reaction with different levels of glucose, which agrees with the linear relationship from 0 mM to 10 mM.

Future utility of the presented chip manufacturing method

For research in private laboratories, the proposed printing system can be reproduced as desktop equipment for the manufacture of microfluidics chips. By leveraging the flexibility and compatibility of inkjet printing, different structures can be achieved by the design of graphics in the CAD software. With this full-printing method, technicians can easily get a chip

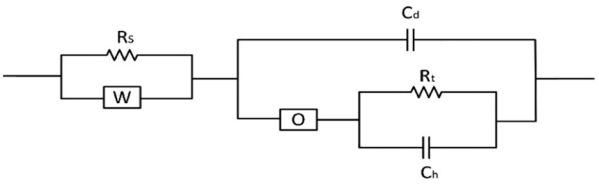

Fig. 6 Equivalent electrical circuit model fitted using Zsimpwin.

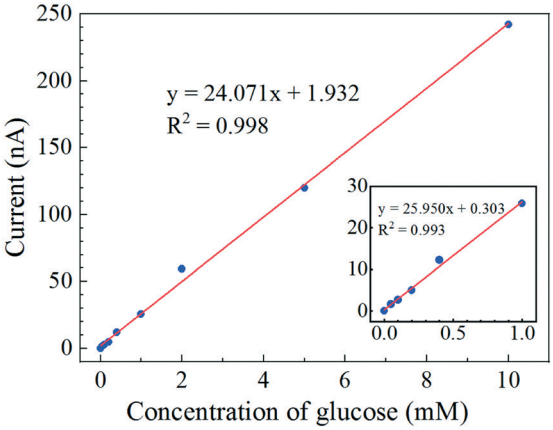

Fig. 7 Result of the measurement with the full-printing glucose sensor (room temperature, 22 °C).

demo, in which the structure of microfluidics is formed by ice instead of the reverse mould and the electrodes are formed by nanoparticle ink instead of electroplating or magnetic sputtering. This method, which gets rid of complicated fabrication processes under ultra-clean room conditions, such as photolithography, remarkably reduces the fabrication cost.

In addition, the full-printing method has great potential in industrial manufacture. Each printing step is independent and can be projected in an assembly line. Taking the glucose sensor in this paper as an example, although it takes nearly an hour to fabricate one chip, at most ten chips could be produced in an hour with four printing systems. The production per hour is only limited by the longest printing step in the whole process.

Conclusions

In this paper, we proposed a cost-effective and time-saving full-printing method based on layer-by-layer inkjet printing, which was appropriate for mass production of chemical biosensors. This method showed good integration capabilities of different materials and structures with different geometries, sizes, heights and layers. By utilizing a commercially available printer and commonly used CAD software, the inkjet printing system significantly reduced the expense of both equipment and technological processing, and can be easily reproduced in private laboratories.

Furthermore, multi-function analysis can be realized by constructing different gel environments in different places and different layers for different targets on one microfluidic chip. Particularly, a more complex structure with more layers in different patterns can be designed to process functions such as extraction, transmission, volume measurement and storage into a highly integrated microfluidic chip.

A glucose detection chip sensor for microfluidic sensing was fabricated successfully using inkjet printing from the functional structure to packaging. So was an integrated lab-on-a-chip system. The system implemented a three-electrode electrochemical sensor and enzyme embedded gel as the biochemical reactor all in one microfluidic chip. The work here

described a new direction for fabricating functionalized microfluidics chips. The full-printing fabrication method might offer potential for application in industrial manufacturing, as the operating mode could be designed into full-automatic flow line production.

Author contributions

F. Y. Zheng, Z. H. Pu and E. Q. He conceived the idea of the study; F. Y. Zheng, Z. H. Pu and J. S. Huang performed the research; Z. H. Pu and B. C. Yu collected and analysed the data; F. Y. Zheng wrote the initial draft of the paper; all authors discussed the results and revised the manuscript.

Conflicts of interest

There are no conflicts to declare.

Acknowledgements

This work was supported by the National Key Research and Development Program of China (No. 2016YFA0200802 and No. 2017YFA0205103) and the National Natural Science Foundation of China (No. 91323304 and No. 81571766)

References

1 G. M. Whitesides, *Nature*, 2006, **442**(7101), 368–373.
2 Y. Zhang, S. Ge and J. Yu, *TrAC, Trends Anal. Chem.*, 2016, **85**, 166–180.
3 J. Wu, Q. Chen, W. Liu, Z. He and J. M. Lin, *TrAC, Trends Anal. Chem.*, 2016, **87**, 19–31.
4 A. C. Glavan, D. C. Christodouleas, B. Mosadegh, H. D. Yu, B. S. Smith, J. Lessing and G. M. Whitesides, *Anal. Chem.*, 2014, **86**(24), 11999–12007.
5 J. M. Pearce, *Science*, 2012, **337**(6100), 1303–1304.
6 Q. Zhang, J. J. Xu, Y. Liu and H. Y. Chen, *Lab Chip*, 2008, **8**(2), 352–357.
7 H. J. Pandya, S. Chandra and A. L. Vyas, *Sens. Actuators, B*, 2012, **161**(1), 923–928.
8 J. T. Feng and Y. P. Zhao, *Biomed. Microdevices*, 2008, **10**(1), 65.
9 Z. Nie, C. A. Nijhuis, J. Gong, X. Chen, A. Kumachev, A. W. Martinez, M. Narovlyansky and G. M. Whitesides, *Lab Chip*, 2010, **10**(4), 477–483.
10 S. Bhattacharya, A. Datta, J. M. Berg and S. Gangopadhyay, *J. Microelectromech. Syst.*, 2005, **14**(3), 590–597.
11 Z. H. Sheng, L. Shao, J. J. Chen, W. J. Bao, F. B. Wang and X. H. Xia, *ACS Nano*, 2011, **5**(6), 4350–4358.
12 X. Li, J. Tian, T. Nguyen and W. Shen, *Anal. Chem.*, 2008, **80**(23), 9131–9134.
13 A. J. Blake, T. M. Pearce, N. S. Rao, S. M. Johnson and J. C. Williams, *Lab Chip*, 2007, **7**(7), 842–849.
14 Z. Pu, C. Zou, R. Wang, X. Lai, H. Yu, K. Xu and D. Li, *Biomicrofluidics*, 2016, **10**(1), 011910.
15 H. Wang, J. Liu, X. Zheng, X. Rong, X. Zheng, H. Peng, Z. Silber-Li, M. Li and L. Liu, *Sci. Rep.*, 2015, **5**, 10945.
16 A. Moya, G. Gabriel, R. Villa and F. J. D. Campo, *Curr. Opin. Electrochem.*, 2017, 29–39.
17 J. Wu, R. Wang, H. Yu, G. Li, K. Xu, N. C. Tien, R. C. Roberts and D. Li, *Lab Chip*, 2015, **15**(3), 690.
18 Z. Pu, R. Wang, J. Wu, H. Yu, K. Xu and D. Li, *Sens. Actuators, B*, 2016, **230**, 801–809.
19 H. Zhang, H. Li, M. Wu, H. Yu, W. Wang and Z. Li, in *IEEE International Conference on MICRO Electro Mechanical Systems*, 2014.
20 G. P. Hicks and S. J. Updike, *Anal. Chem.*, 1966, **38**(6), 726.
21 Z. P. Fengyi Zheng, E. He, D. Li and Z. Li, in *The 21st International Conference on Miniaturized Systems for Chemistry and Life Sciences (MicroTAS 2017)*, Savannah, USA, 2017, p. 761.
22 A. Asai, M. Shioya, S. Hirasawa and T. Okazaki, *J. Imaging Sci. Technol.*, 1993, **37**(Suppl 6), 205–207.
23 M. S. Khan, D. Fon, X. Li, J. Tian, J. Forsythe, G. Garnier and W. Shen, *Colloids Surf., B*, 2010, **75**(2), 441–447.

